General Disclaimer

One or more of the Following Statements may affect this Document

- This document has been reproduced from the best copy furnished by the organizational source. It is being released in the interest of making available as much information as possible.

- This document may contain data, which exceeds the sheet parameters. It was furnished in this condition by the organizational source and is the best copy available.

- This document may contain tone-on-tone or color graphs, charts and/or pictures, which have been reproduced in black and white.

- This document is paginated as submitted by the original source.

- Portions of this document are not fully legible due to the historical nature of some of the material. However, it is the best reproduction available from the original submission.

AN ANALYTICAL METHOD FOR PREDICTING THE LIFT AND DRAG FOR SLENDER

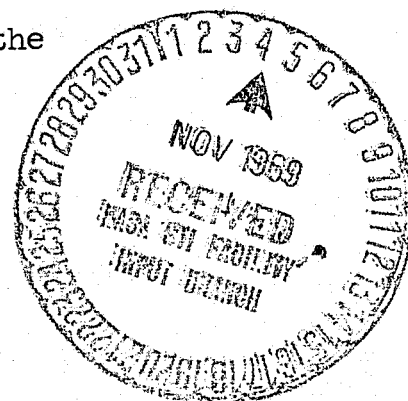SHARP-EDGE DELTA WINGS IN GROUND PROXIMITY

By

Charles Harry Fox, Jr.

Thesis submitted to the Graduate Faculty of the

Virginia Polytechnic Institute

in candidacy for the degree of

MASTER OF SCIENCE

in

Aerospace Engineering

March 1969

AN ANALYTICAL METHOD FOR PREDICTING THE LIFT AND DRAG FOR SLENDER SHARP-EDGE DELTA WINGS IN GROUND PROXIMITY

By

Charles Harry Fox, Jr.

ABSTRACT

A potential flow lifting surface method is combined with a vortex lift concept and applied to slender sharp-edge delta wings. A multihorseshoe vortex lattice method incorporating an image technique is used to compute the potential flow normal force and axial force characteristics of delta wings in ground proximity. A free-air vortex lift concept based on a leading edge suction analogy is utilized to account for the lift increment due to the leading edge spiral vortex. A method is developed for combining the free air vortex lift concept with the potential flow theory results in ground proximity.

A comparison of theoretical and experimental lift and drag for delta wings having a wide range of aspect ratios is made at selected angles of attack. The comparison indicates that this method provides a reasonably good prediction of the lift and drag in ground proximity for aspect ratios less than two in the angle of attack range from approximately 5° to 16°.

AN ANALYTICAL METHOD FOR PREDICTING THE LIFT AND DRAG FOR SLENDER

SHARP-EDGE DELTA WINGS IN GROUND PROXIMITY

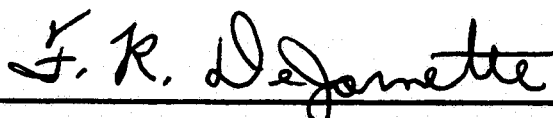by

Charles Harry Fox, Jr.

Thesis submitted to the Graduate Faculty of the

Virginia Polytechnic Institute

in partial fulfillment for the degree of

MASTER OF SCIENCE
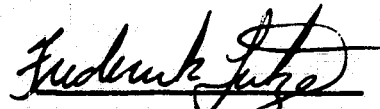
in

Aerospace Engineering

APPROVED: _____
Chairman, F. R. DeJarnette

_____
F. O. Bunting, Ph. D
Professor of Aerospace Engineering
University of Virginia

_____
F. H. Lutze

March 1969

Blacksburg, Virginia

II. TABLE OF CONTENTS

III. <u>ACKNOWLEDGEMENTS</u>

IV. LIST OF FIGURES

V. INTRODUCTION*

In the design of large aircraft, it is important to consider the effect of ground proximity on the aerodynamic characteristics because significant alterations in these characteristics may occur during take-off and landing (ref. 2). The present study is concerned with aircraft having delta wings with sharp leading edges, low aspect ratio, and thin, planar airfoil sections and is restricted to the consideration of the isolated wing only. The present study develops a method for the prediction of the effect of ground proximity on the lift and drag of these wings.

Classical potential flow theory as implemented by lifting line and horseshoe vortex methods (ref. 3) has proven inadequate to predict the lift and drag of the low aspect ratio, sharp leading edge delta wing irrespective of the presence of the ground. One reason for this inadequacy is the failure of these methods to treat the chordwise variation of lift. Lifting surface theory using vortex lattice methods (refs. 4 and 5) was developed in order to include the chordwise lift distribution; however, even these techniques are inadequate to treat the present planform. The basic reason is that classical potential theory assumes completely attached flow while, in the real flow, the flow separates from the sharp leading edges and forms spiral vortices which result in a loss of leading edge suction and an increase in lift.

A new concept of the vortex lift of planar sharp leading edge delta wings based on a leading edge suction analogy is presented in reference 6. This concept provides a reasonably accurate method of predicting the total lift of planar sharp edge delta wings in the absence of the ground.

*The material in this thesis is also presented in reference 1.

The present study employs a vortex lattice potential flow theory lifting surface method incorporating an image technique to represent the wing in ground proximity and a method is introduced for combining it with the free air vortex lift concept. The resulting theory yields a reasonably good prediction of the total lift and drag of sharp edge planar wings in ground proximity. Note that the method is not applicable to the prediction of pitching moment. Therefore, the present study is restricted to the consideration of lift and drag.

VI. SYMBOLS

A	axial force, positive toward trailing edge
AR	aspect ratio, b^2/S
B	matrix defined by equation (9)
b	total wing span, ft(m)
C_A	axial force coefficient, axial force/qS, positive toward trailing edge
$C_{A,der}$	axial force coefficient derived from $C_{N,lat}$, $C_{A,lat}$, and $\partial C_{D_i}/\partial C^2_{L,lat}$
C_D	drag coefficient, drag/qS
$\partial C_{D_i}/\partial C^2_{L,lat}$	induced drag factor
C_L	lift coefficient, lift/qS
$C_{L,v}$	lift coefficient associated with leading edge vortex
C_N	normal force coefficient, normal force/qS, positive away from ground plane
$C_{N,v}$	normal force coefficient associated with leading edge vortex
C_S	leading edge suction coefficient (in plane of wing and perpendicular to leading edge)
C_T	leading edge thrust coefficient (in plane of wing and parallel to flight direction)
$\bar{c}$	mean aerodynamic chord
H	influence coefficient
h	height of apex of wing above ground

3

$\dfrac{h_{\overline{c}/4}}{\overline{c}}$ normalized height parameter, height of the quarter chord

of the mean aerodynamic chord divided by the mean

aerodynamic chord

K a free air proportional correction to the vortex lattice

axial force coefficient defined as $C_{A,der}/C_{A,lat}$

l length

N normal force, positive away from ground

n normal distance defined in figure 2

$P(x,y,z)$ a general point in space

q dynamic pressure, lb/ft^2, (N/m^2)

S wing reference area, ft^2 (m^2)

s horseshoe vortex semispan

U_∞ free-stream velocity, $U_\infty = 1$

V resultant velocity with components u,v,w

u,v,w perturbation velocity components in the positive X,Y,Z

directions

X,Y,Z orthogonal right-handed primary Cartesian coordinate

system with origin at the wing apex (see fig. 1(c)),

positive X is away from the trailing edge, positive Y

is toward the right wing tip, positive Z is toward

the ground plane

X^*,Y^*,Z^* orthogonal right-handed primary coordinate system

associated with image wing, (see fig. 1(d)), positive X^*

is away from trailing edge, positive Y^* is parallel

to positive Y

x,y,z	orthogonal right-handed secondary Cartesian coordinate system with origin at the lateral midpoint of the local quarter chord of an element (see fig. 1(b))
x^*,y^*,z^*	orthogonal right-handed secondary coordinate system associated with image wing
α	angle of attack, deg
Γ	circulation strength
δ	angle defined in figure 2
φ	angle between normal to ground plane and Z-axis, deg, note that $\varphi = \alpha$
ψ	angle between bound vortex and y-axis, deg, positive direction is counterclockwise from positive y-axis
θ	angle defined in figure 2
Λ	leading edge sweep angle, deg

Subscripts

a	a particular point $P_a(x_a,y_a,z_a)$
b	a particular point $P_b(x_b,y_b,z_b)$
BC	boundary condition
c	chordwise segment
I	image wing
l	left wing panel
lat	potential flow theory vortex lattice computer program results
min	minimum
p	potential flow theory assuming zero leading edge suction

pot   potential flow theory using $C_{A,der}$

R   real or actual wing

r   right wing panel

s   spanwise segment

t   total

u,v,w   components of influence coefficient in x,y,z directions

VII. POTENTIAL FLOW THEORY (VORTEX LATTICE THEORY)

The basis for the implementation of the potential flow theory in the present study is the ability to represent a lifting wing by a series of horseshoe vortices. The vortex lattice method represents both the spanwise and the chordwise distribution of lift by a system of horseshoe vortices. The wing is divided into elemental parts, each of which is represented by a horseshoe vortex and a control or boundary point. A simplified subdivision of a delta wing into elemental parts is shown in figure 1(a). A horseshoe vortex representing a typical element is shown in figure 1(b).

The orthogonal primary coordinate system used for the wing is shown in figure 1(c). The height of the wing apex above the ground is h. The angle between h and the Z-axis is φ. The angle of attack is defined as the angle between the free-stream velocity and the X-axis. The perturbation velocities in the X, Y, and Z-directions are shown in figure 1(c) as u, v, and w, respectively.

To simplify the analysis, the assumption is made that $\varphi = \alpha$. Thus, the present investigation does not attempt to represent the dynamic situation of an aircraft landing maneuver in which φ and α are independent functions of time.

The orthogonal secondary coordinate system associated with the horseshoe vortex, representing a typical element of the wing, is shown in figure 1(b). Note that a secondary coordinate system is associated with each horseshoe vortex of the lattice.
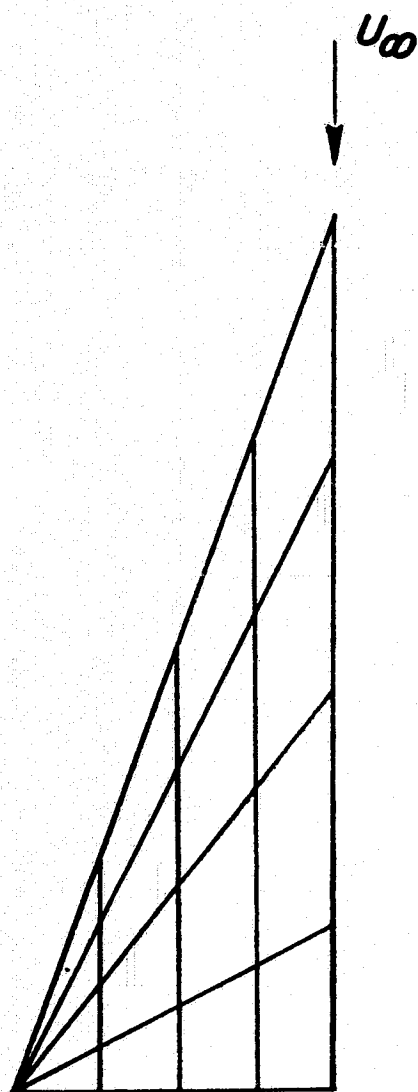
(a) Simplified subdivision of
    left wing panel.
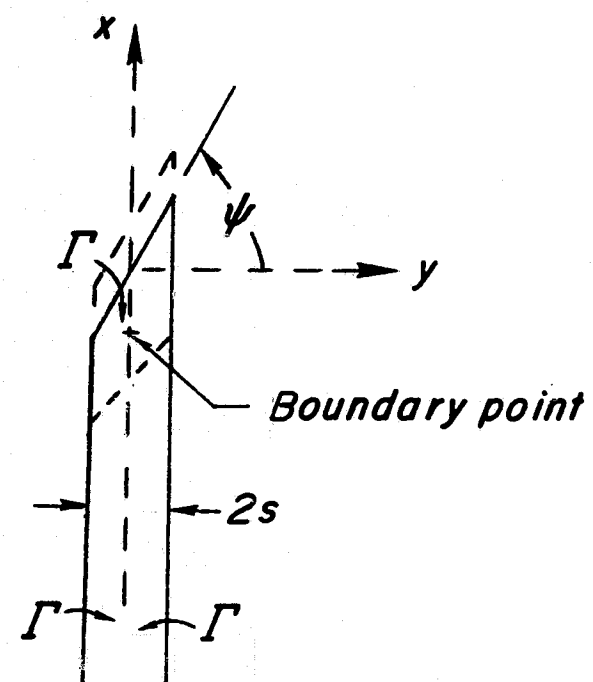
(b) Typical horseshoe vortex layout.

Figure 1.- Application of vortex lattice to delta wing.

(c) Geometry associated with real wing.

Figure 1.- Continued.

$P_b (X_b', Y_b', 0)$

$X_b \cos 2\phi$

X

$X_b \sin 2\phi$

Real wing

ϕ

2ϕ

+Y is out of paper

$2h \sin \phi$

Z

h

Trailing wakes

Ground plane

$2h \cos \phi$

h

$P_a (X_a, Y_a, 0)$

Image wing

ϕ

X^*

+Y* is out of paper

Z^*
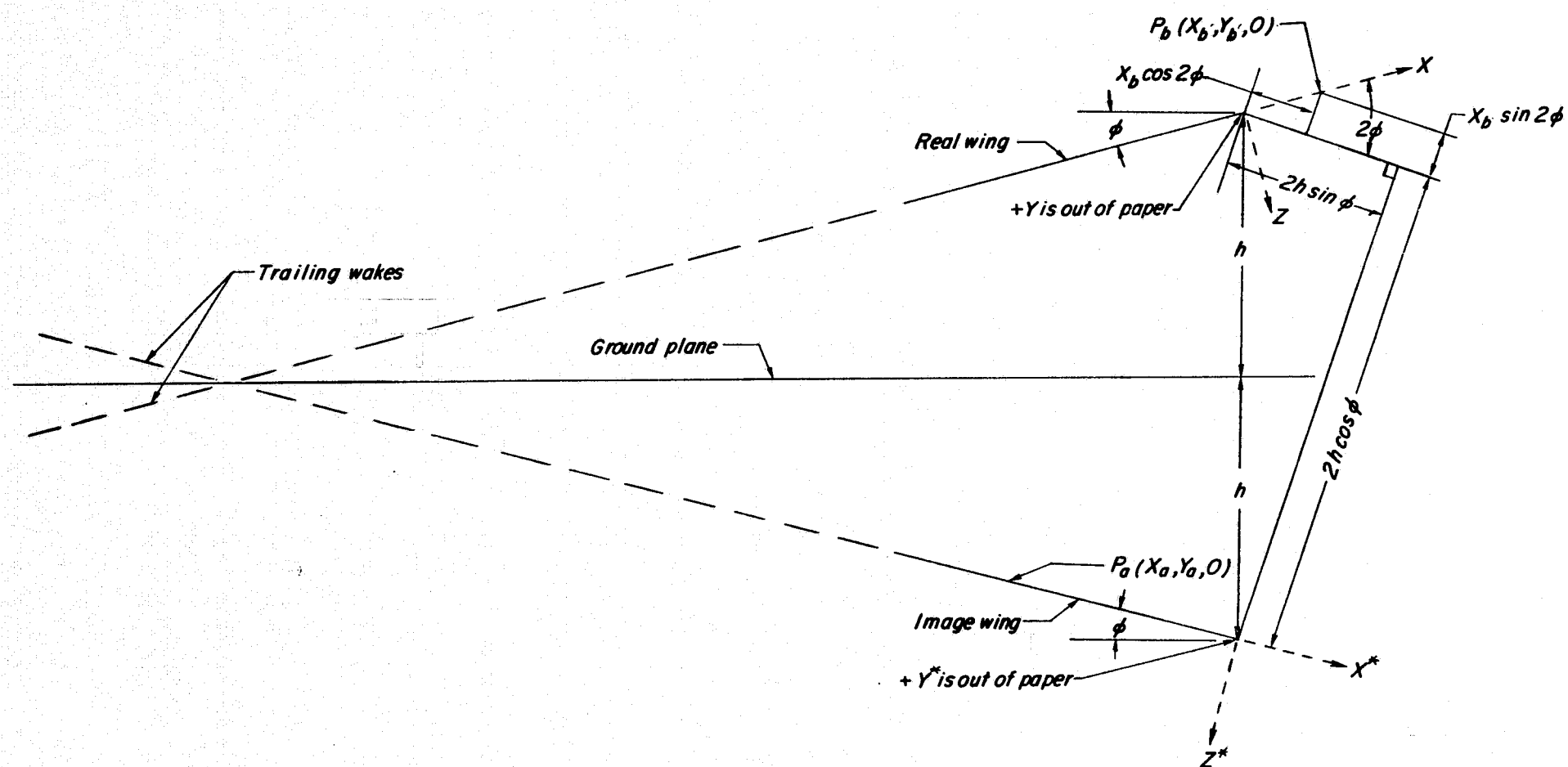
(d) Coordinate systems associated with real and image wings.

Figure 1.- Concluded.

A second primary coordinate system (fig. 1(d)) is associated with the image wing. Note the positive directions in the two primary coordinate systems.

The basic relation between the velocities and the horseshoe vortex circulation strengths is, in matrix notation:

$$\{V\} = [H]\{\Gamma\} \tag{1}$$

where H is a geometric influence coefficient matrix (see ref. 7). In the computer program, this vector equation is replaced by three scalar equations for u, v, and w.

In order to compute the influence coefficient, the law of Biot-Savart is applied. This law, as originally derived in electromagnetic field theory, says that the magnetic field intensity in the neighborhood of a long straight wire carrying a steady current varies inversely as the radial distance to the wire (see ref. 8). The analogy between electromagnetic theory and vortex flow is discussed by Lamb (see ref. 9, section 148). Following reference 7, pages 127-128, the velocity induced at a point by a finite line of vorticity is given by

$$V = H\Gamma = \frac{1}{4\pi m}(\cos \delta + \cos \theta)\Gamma \tag{2}$$

where the symbols are defined in figure 2.

A more general situation must be considered in the present problem as shown in figure 3. The influence of a complete horseshoe vortex (line BAA'B') on the induced velocity at a general point (P) in three
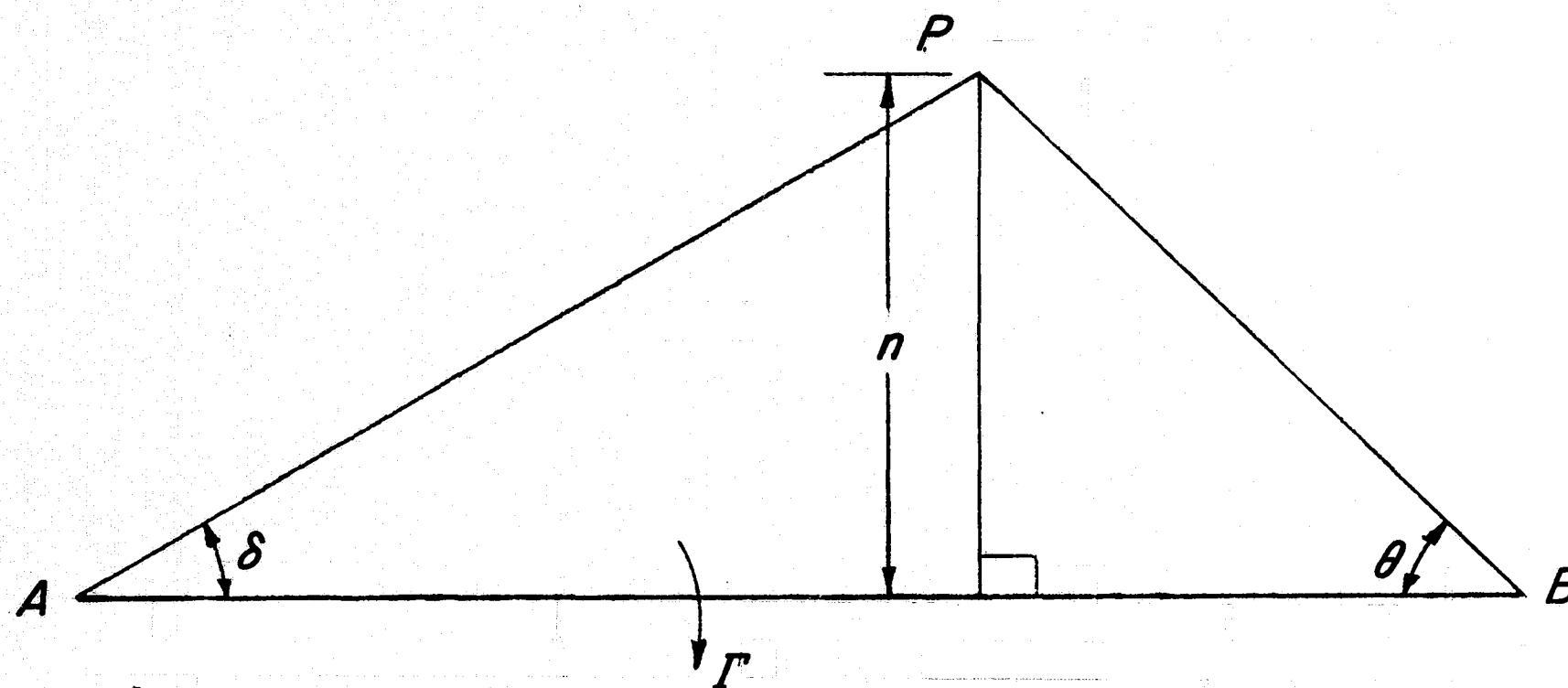
Figure 2.- Geometry for a single finite line vortex.

$$\overline{PN} \perp \overline{AB}$$
$$\overline{PN'} \perp \overline{AB'}$$
$$\overline{PQ} \perp \overline{A'M'}$$
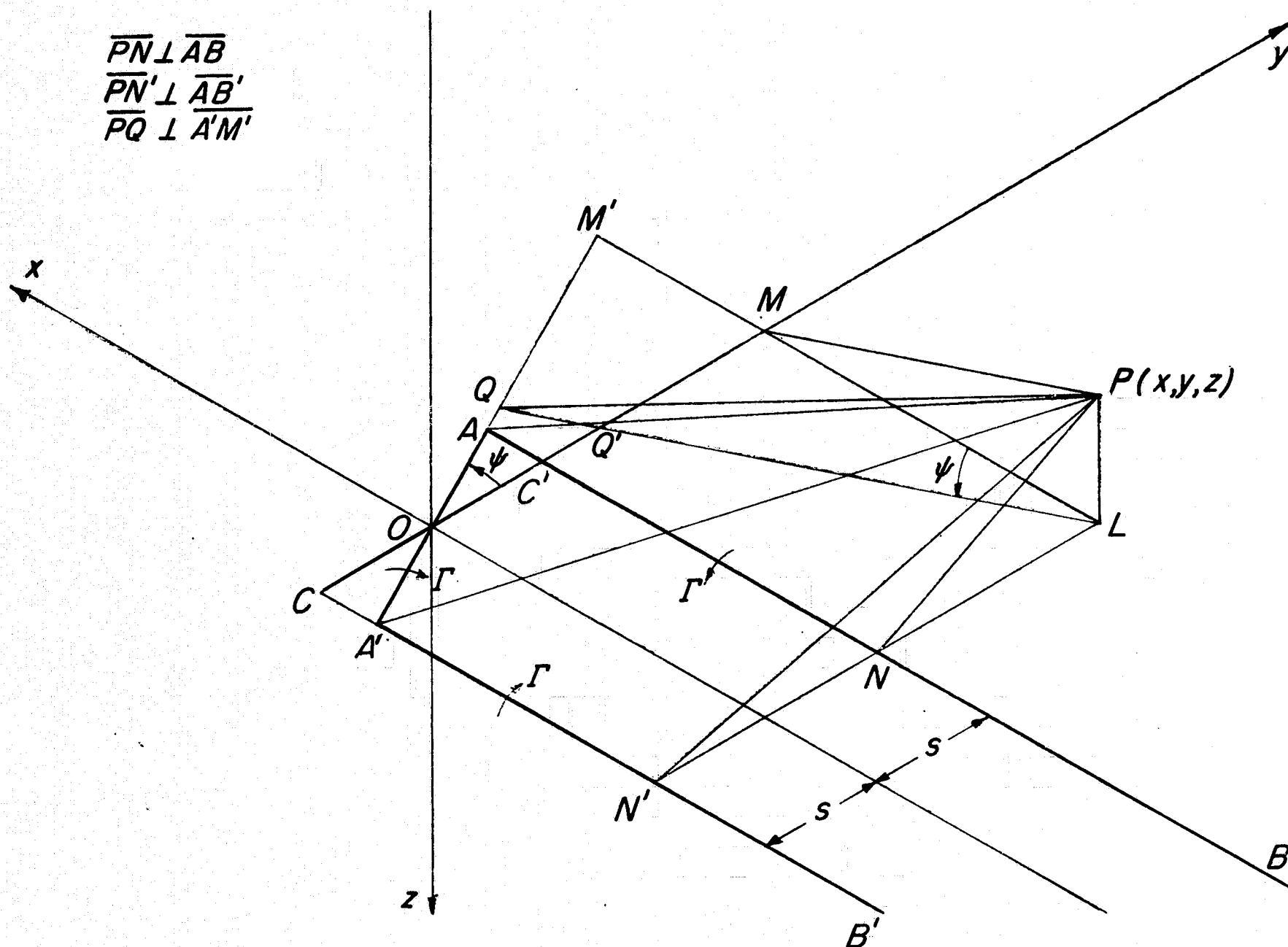
Figure 3.- Geometry for a horseshoe vortex.

13

dimensional space must be computed. In the figure note that the trailing vortex legs (AB and A'B') actually extend to infinity. Applying equation (2) to each part of the horseshoe vortex in figure 3, the equation for H becomes

$$H = \frac{1}{4\pi\overline{PQ}}(\cos \angle PAA' + \cos \angle PA'A)$$

$$+ \frac{1}{4\pi\overline{PN}'}(\cos \angle PB'A' + \cos \angle PA'B')$$

$$+ \frac{1}{4\pi\overline{PN}}(\cos \angle PBA + \cos \angle PAB) \tag{3}$$

which reduces to

$$H = \frac{1}{4\pi\overline{PQ}}\left(\frac{\overline{AQ}}{\overline{PA}} + \frac{\overline{A'Q}}{\overline{PA'}}\right) + \frac{1}{4\pi\overline{PN}'}\left(1 + \frac{\overline{AN}}{\overline{PA}}\right) + \frac{1}{4\pi\overline{PN}}\left(1 + \frac{\overline{A'N'}}{\overline{PA'}}\right) \tag{4}$$

Note that for clarity the angles $\angle$ PB'A' and $\angle$ PBA are not shown in the figure since B' and B represent points at infinity and therefore the angles are zero and the corresponding cosines are unity as given in equation (4).

Omitting the algebra (fig. 3 includes all geometric constructions used in performing the algebra) and recalling that in the present problem the vector equation is broken up into three scalar equations, the scalar influence coefficients are given by the following equations

$$H_u(x,y,z) = \left\{ \frac{z \cos \psi}{4\pi\left[z^2 + (y \sin \psi - x \cos \psi)^2\right]} \right\} \left[\frac{y \cos \psi + x \sin \psi + \dfrac{s}{\cos \psi}}{\sqrt{z^2 + (y+s)^2 + (x+s \tan \psi)^2}} - \frac{y \cos \psi + x \sin \psi - \dfrac{s}{\cos \psi}}{\sqrt{z^2 + (y-s)^2 + (x-s \tan \psi)^2}} \right]$$

<div align="right">(5(a))</div>

$$H_v(x,y,z) = \left\{ \frac{- z \sin \psi}{4\pi\left[z^2 + (y \sin \psi - x \cos \psi)^2\right]} \right\} \left[\frac{y \cos \psi + x \sin \psi + \dfrac{s}{\cos \psi}}{\sqrt{z^2 + (y+s)^2 + (x+s \tan \psi)^2}} - \frac{y \cos \psi + x \sin \psi - \dfrac{s}{\cos \psi}}{\sqrt{z^2 + (y-s)^2 + (x-s \tan \psi)^2}} \right]$$

$$+ \left\{ \frac{z}{4\pi\left[z^2 + (y-s)^2\right]} \right\} \left[1 + \frac{-x + s \tan \psi}{\sqrt{z^2 + (y-s)^2 + (x-s \tan \psi)^2}} \right]$$

$$+ \left\{ \frac{-z}{4\pi\left[z^2 + (y+s)^2\right]} \right\} \left[1 + \frac{-x - s \tan \psi}{\sqrt{z^2 + (y+s)^2 + (x+s \tan \psi)^2}} \right]$$

<div align="right">(5(b))</div>

$$H_w(x,y,z) = \left\{ \frac{y \sin \psi - x \cos \psi}{4\pi \left[z^2 + (y \sin \psi - x \cos \psi)^2 \right]} \right\} \left[\frac{y \cos \psi + x \sin \psi + \dfrac{s}{\cos \psi}}{\sqrt{z^2 + (y+s)^2 + (x+s \tan \psi)^2}} - \frac{y \cos \psi + x \sin \psi - \dfrac{s}{\cos \psi}}{\sqrt{z^2 + (y-s)^2 + (x-s \tan \psi)^2}} \right]$$

$$+ \left\{ \frac{-(y-s)}{4\pi \left[z^2 + (y-s)^2 \right]} \right\} \left[1 + \frac{-x + s \tan \psi}{\sqrt{z^2 + (y-s)^2 + (x - s \tan \psi)^2}} \right]$$

$$+ \left\{ \frac{y+s}{4\pi \left[z^2 + (y+s)^2 \right]} \right\} \left[1 + \frac{-x - s \tan \psi}{\sqrt{z^2 + (y+s)^2 + (x + s \tan \psi)^2}} \right] \qquad (5(c))$$

Equations (5) are based on the assumption that the trailing vortex sheet lies in the plane of the wing and extends to infinity. The physical situation in which the trailing vortex sheet essentially follows the free-stream direction is not represented because this assumption was made. Nonetheless, this assumption was made in order to simplify the equations.

In the present case, it is necessary to consider the complete vortex lattice. From considerations of symmetry, for each horseshoe vortex on the left half of the real wing, there exists a corresponding horseshoe vortex on the right half of the real wing as well as on the left and right halves of the image wing, all of which have equal circulation strengths. Therefore, equation (1) can be restricted to consideration of the left half of the real wing provided each element of the H matrix is the sum of four successive applications of equations (5) with sets of the secondary coordinates (x,y,z) appropriate to each of the four wing panels being used.

Let $(X_b, Y_b, 0)$ represent the coordinate of a point P_b on the left half of the real wing at which induced velocities are to be computed. Let $(X_a, Y_a, 0)$ be the origin of the secondary coordinate system of a horseshoe vortex on the left half of the real wing. The corresponding element of the influence-coefficient matrix $\begin{bmatrix} H \end{bmatrix}$ may be written as

$$H = H_{l,R} + H_{r,R} + H_{l,I} + H_{r,I} = H_R + H_I \qquad (6)$$

The u, v, and w components of $H_{l,R}$ are found directly from equations (5) by letting $y = y_l$ and using

$$x = X_b - X_a$$

$$y_l = Y_b - Y_a$$

$$z = 0$$

Since $H_{r,R}$ is symmetrically related to the influence of the left real horseshoe vortex on a point $(X_b, -Y_b, 0)$, let $y_r = -Y_b - Y_a$ and reverse the sign of the component of V in the Y-direction. Then, the components of $H_R = H_{l,R} + H_{r,R}$ are

$$H_{u,R} = H_u(x, y_l, z) + H_u(x, y_r, z) \qquad (7(a))$$

$$H_{v,R} = H_v(x, y_l, z) - H_v(x, y_r, z) \qquad (7(b))$$

$$H_{w,R} = H_w(x, y_l, z) + H_w(x, y_r, z) \qquad (7(c))$$

To determine the image-wing influence terms, the X,Y,Z coordinate system is translated downward through the ground plane and rotated through an angle of 2φ in the XZ-plane. (See figure 1(d).) The assumption

that the wake of the real wing lies in the XY-plane results in a wake which, at positive angles of attack, intercepts the ground and passes into the image region below. Similarly, the image wake intercepts the ground and passes into the real region above. Although it is hoped that such behavior will not significantly affect the present results, large errors would probably result if the present technique were used to obtain the downwash at a rear tail. The technique used to form the image in this investigation depends upon the assumption that the wing is planar. The image system would be incorrect if the wing had such nonplanar characteristics as camber, twist, dihedral, or a deflected flap.

With respect to the $X*,Y*,Z*$ coordinate system, the coordinates of the point $(X_b,Y_b,0)$ become (see fig. 1(d))

$$X_b^* = -2h \sin \varphi + X_b \cos 2\varphi$$

$$Y_b^* = Y_b$$

$$Z_b^* = -2h \cos \varphi - X_b \sin 2\varphi$$

Thus, to obtain the influence of the left half of the image wing on the left half of the real wing $(H_{l,I})$, use

$$x^* = -2h \sin \varphi + X_b \cos 2\varphi - X_a$$

$$y_1^* = Y_b - Y_a$$

$$z^* = 2h \cos \varphi - X_b \sin 2\varphi$$

To obtain the influence of the right half of the image wing on the left half of the real wing, the y-coordinate is altered to

$$y_r^* = - Y_b - Y_a$$

and the sign of the v component is reversed.

Substitution of these coordinates into equations (5) yields the components H_u^*, H_v^*, and H_w^*. These image-influence components are expressed in the directions of the rotated axis system. The following equations are used to resolve the image influence into the X-, Y-, and Z-directions and to account for the fact that the circulation strengths of the image vortices are opposite in sense to those on the real wing:

$$\left[H_I \right] = - \left[B \right] \left[H^* \right] \tag{8}$$

where

$$H_I = \quad H_{l,I} + H_{r,I}$$

and the components of the H_I matrix are $H_{u,I}$, $H_{v,I}$, and $H_{w,I}$; the components of the H* matrix are H_u^*, H_v^*, and H_w^*; and the B matrix is defined as follows:

$$B = \begin{bmatrix} \cos 2\varphi & 0 & -\sin 2\varphi \\ 0 & 1 & 0 \\ \sin 2\varphi & 0 & \cos 2\varphi \end{bmatrix} \tag{9}$$

Since only planar wings are considered in the present study, the boundary condition is

$$w_{BC} - U_\infty \sin \alpha = 0 \tag{10}$$

or for a free-stream velocity of unity

$$w_{BC} = \sin \alpha \tag{11}$$

The circulation strengths are then computed from the equation

$$\{\Gamma\} = [H]^{-1}\{w_{BC}\} \tag{12}$$

where each element of the H matrix is the total influence at a given boundary point caused by a given set of four symmetrically placed vortices on the real and image wings.

Since the circulation strengths are known, computation of the forces acting on the wing is now possible. Let a segment be defined as that portion of a line of vorticity on the wing which has a constant circulation strength. The present analysis computes the induced velocity at the midpoint of each segment from the equation

$$\{v\} = [H]\{\Gamma\} \tag{13}$$

where the H matrix is now the influence of the set of horseshoe vortices on the set of points composed of the midpoints of the segments. If the induced velocities are expressed in terms of u, v, and w, then the forces on the wing can be computed by forming the vector cross product of the circulation strengths of the segments and the induced velocities at the midpoints of the segments. For a spanwise segment, the forces are

$$F_{A,s} = 2\Gamma_s(w_s - \sin \alpha)(2s) \tag{14}$$

$$F_{N,s} = 2\Gamma_s\left[v_s \tan \psi - (u_s - \cos \alpha)\right](2s) \tag{15}$$

where the subscript s denotes a spanwise segment. For a chordwise segment, the forces are

$$F_{A,c} = 0 \qquad\qquad (16)$$

$$F_{N,c} = 2\Gamma_c v_c l_c \qquad\qquad (17)$$

where the subscript c denotes a chordwise segment, l_c is the segment length contained within the planform, and Γ_c is the net circulation strength resulting from the individual circulations of each trailing-horseshoe-vortex leg forming that segment.

The total normal and axial forces acting on the wing are obtained by summing the normal and axial forces acting on all segments.

The preceding system of equations have been programed for solution on a high speed digital computer. The results from this computer program are referred to as the vortex lattice theory. The vortex lattice theory lift and drag coefficients are therefore given as:

$$C_{L,lat} = C_{N,lat} \cos \alpha - C_{A,lat} \sin \alpha \qquad\qquad (18(a))$$

$$C_{D,lat} = C_{N,lat} \sin \alpha + C_{A,lat} \cos \alpha \qquad\qquad (18(b))$$

An axial-force coefficient $C_{A,lat}$ can be calculated by using the vortex-lattice method as implemented herein since the total velocities used to compute the forces on the vortex lines were calculated at the midpoint of each vortex segment rather than at the control point where the boundary condition was applied. However, the values obtained are somewhat inaccurate because of the discrete nature of the vortex-lattice formulation of the problem. The first task is, therefore, the correction of the axial-force coefficient. The method used relies on the fact that the vortex-lattice span load distribution in free air can be used to compute an

accurate value of the induced-drag factor $\dfrac{\partial C_{Di}}{\partial c^2_{L,lat}}$. The accuracy of this

calculation has been checked by independent methods. (See reference 10.)

Thus, a better approximation of the free-air axial-force coefficient, valid

for large angles of attack in potential flow, is obtained from the

solution of

$$- C_{A,der} = C_{L,lat} \sin \alpha - \frac{\partial C_{Di}}{\partial c^2_{L,lat}} c^2_{L,lat} \cos \alpha \tag{19}$$

$$C_{L,lat} = C_{N,lat} \cos \alpha - C_{A,der} \sin \alpha$$

The corrected axial-force coefficient in free air may be written in terms

of the vortex-lattice axial-force coefficients as

$$C_{A,der} = KC_{A,lat} \tag{20}$$

Equation (20) defines K, the fractional correction to the free air axial-

force coefficient. It is assumed that, for a given wing planform, K is

a function of angle of attack but not a function of height above the

ground.

The effect of introducing K is to replace equations (18) by

$$C_{L,pot} = C_{N,lat} \cos \alpha - KC_{A,lat} \sin \alpha \tag{21(a)}$$

$$C_{D,pot} = C_{N,lat} \sin \alpha + KC_{A,lat} \cos \alpha \tag{21(b)}$$

Results obtained from use of these equations are referred to as the

potential theory lift and drag coefficients.

VIII. VORTEX LIFT CONCEPT

The potential flow theory as developed in the preceding section can not be applied to sharp leading edge wings. The reason for this is that the potential flow theory is based on the assumption of full leading edge suction whereas for the slender sharp leading edge low aspect ratio delta wing of the present study, the leading edge suction is lost and a leading edge spiral vortex is formed. Reference 6 presents a new concept of the free air vortex lift of sharp edge delta wings based on a leading edge suction analogy. Since the present theory to be discussed below is based on a combination of the potential flow theory and the vortex lift concept, an understanding of the vortex lift concept is important to the understanding of the present theory. Therefore, the following discussion of the vortex lift concept based on reference 6 is presented.

For sharp leading edge low aspect ratio delta wings, the flow separates from the leading edges even at low angles of attack and rolls up into two spiral vortex sheets. The flow reattaches to the upper wing surface inboard of the vortex sheets. This flow pattern results in an increase in lift at a given angle of attack and is referred to as non-linear or vortex lift. The vortex lift concept assumes that the total lift can be calculated from a potential flow lift and a lift associated with the leading edge spiral vortices.

The potential flow lift for the zero leading edge suction condition is given by

$$C_{L,p} = C_{N,lat} \cos \alpha \qquad (22)$$

The leading edge suction coefficient is simply related to the leading edge thrust coefficient by:

$$C_S = \frac{C_T}{\cos \Lambda} \tag{23}$$

The vortex lift concept asserts that a force is required to maintain the equilibrium of the flow over the spiral vortex assuming the flow reattaches to the wing. The magnitude of this equilibrium force is equal to the magnitude of the potential flow theory leading edge suction force (ref. 6). The vortex lift concept can then be interpreted as a rotation of the resultant suction force into the normal force direction and thus the normal force coefficient associated with the leading edge vortex is

$$C_{N,v} = \left| C_S \right| \tag{24}$$

The lift coefficient associated with the leading edge vortex is

$$C_{L,v} = C_{N,v} \cos \alpha = \left| C_T \right| \frac{\cos \alpha}{\cos \Lambda} \tag{25}$$

Noting that $\left| C_T \right| = \left| C_{A,lat} \right|$, the above equation can be rewritten as

$$C_{L,v} = \left| C_{A,lat} \right| \frac{\cos \alpha}{\cos \Lambda} \tag{26}$$

The total lift coefficient based on the vortex lift concept is then

$$C_{L,t} = \left(C_{N,lat} + \frac{\left| C_{A,lat} \right|}{\cos \Lambda} \right) \cos \alpha \tag{27(a)}$$

Since zero leading edge suction was assumed, the total drag coefficient becomes

$$C_{D,t} = C_{L,t} \tan \alpha \qquad (27(b))$$

IX. METHOD OF COMBINING POTENTIAL THEORY AND VORTEX LIFT CONCEPT IN GROUND PROXIMITY

Several facets of the preceding analysis led to the idea that the potential flow theory and the vortex lift concept could be combined to permit the prediction of the lift and drag of sharp edge delta wings in ground proximity. The use of the vortex lift concept (eqs. (27)) in free air provided a reasonably good prediction of the characteristics of these wings (as shown in ref. 6). The potential flow theory described in section VII provides a method of computing the variation of normal and axial force for a wing in ground proximity. Finally, the vortex lift concept can be interpreted as a modification to the potential flow theory normal and axial force to account for the leading edge spiral vortices. A straightforward application of the equations presented in the preceding sections leads to the following equations.

$$C_{L,t} = \left(C_{N,lat} + \frac{K |C_{A,lat}|}{\cos \Lambda} \right) \cos \alpha \qquad (28(a))$$

$$C_{D,t} = C_{L,t} \tan \alpha \qquad (28(b))$$

These equations are referred to as the present theory. Note that the assumption that K is independent of ground height and the fact that the vortex lattice method allows one to compute $C_{N,lat}$ and $C_{A,lat}$ as functions of angle of attack and ground height permits equations (28) to be used to compute the total lift and drag in ground proximity. Thus these equations represent a method of combining the potential flow theory in ground proximity with the free air vortex lift concept.

26

X. COMPARISON WITH EXPERIMENT

Several features of the analysis should be noted. First, the existence of the spiral vortices emanating from the leading edge implies a redistribution of vorticity in the wing and wake. This redistribution is not accounted for with respect to the image wing below the ground plane, even though the results of reference 6 have been used to correct for this effect at the real wing. Secondly, the choice of the coordinate system used in the vortex lattice method described in section VII leads to a wake which, at positive angles of attack, intersects and passes through the ground plane. Finally, since the present approach uses the method of reference 6, which does not predict the distribution of forces over the wing, this approach cannot be used to calculate pitching moment.

In view of the assumptions used in developing the present theory, the justification for its use must rest primarily upon a comparison with experimental data. One of the most complete experimental studies of ground effect for sharp-edge delta wings is that of reference 11, in which a series of wings with leading-edge sweep angles of 75°, 70°, 60°, and 50° (aspect ratios of 1.072, 1.456, 2.309, and 3.356, respectively) were tested. These wings were tested by using both the fixed-ground-board and image-model test methods at a free-stream velocity of 114.8 ft/sec (35.0 m/sec) mounted on a strut support. Certain unexplained nonlinearities existed at low angles of attack in the data of reference 11; however, the data were self-consistent. Corresponding with the assumptions of the theory, the wings were isolated; that is, there was no fuselage or tail. The experimental data are presented in terms of the height parameter used

in the present study. Details of the lattice layout used are given in reference 1.

The lift and drag characteristics of the wings as functions of normalized ground height are presented in figure 4 for $\alpha = 10^\circ$, and in figure 5 for $\alpha = 15^\circ$. The drag coefficients presented in these figures do not include the friction-drag component which has been removed by subtracting the minimum drag coefficients from the data of reference 11. (The values subtracted were 0.008, 0.010, 0.011, and 0.012 for wings with leading-edge sweeps of 75°, 70°, 60°, and 50°, respectively.)

An examination of figures 4 and 5 reveals that when either the potential theory or the present theory is able to predict the free-air lift coefficients, it can also be used to predict the effect of ground proximity reasonably well. For aspect ratios less than 2.0, where the leading-edge vortex is well developed, the present theory (eqs. (28)) accurately predicts the lift. As the aspect ratio increases and the effects of the leading-edge vortex become less pronounced, the accuracy of the potential-theory lift predictions (eqs. (21)) becomes progressively better and that of the present-theory predictions becomes worse. In general, the present theory yields a better drag prediction than the potential theory. These effects can also be seen in figures 6 and 7 which summarize the lift and drag characteristics as functions of aspect ratio for selected ground heights.

The potential flow theory prediction, for the lowest aspect ratio presented in figure 6, is only 71 to 77 percent of the lift and 30 percent of the drag compared to a prediction by the present theory of 92 to 100 percent of the lift and 100 percent of the drag.
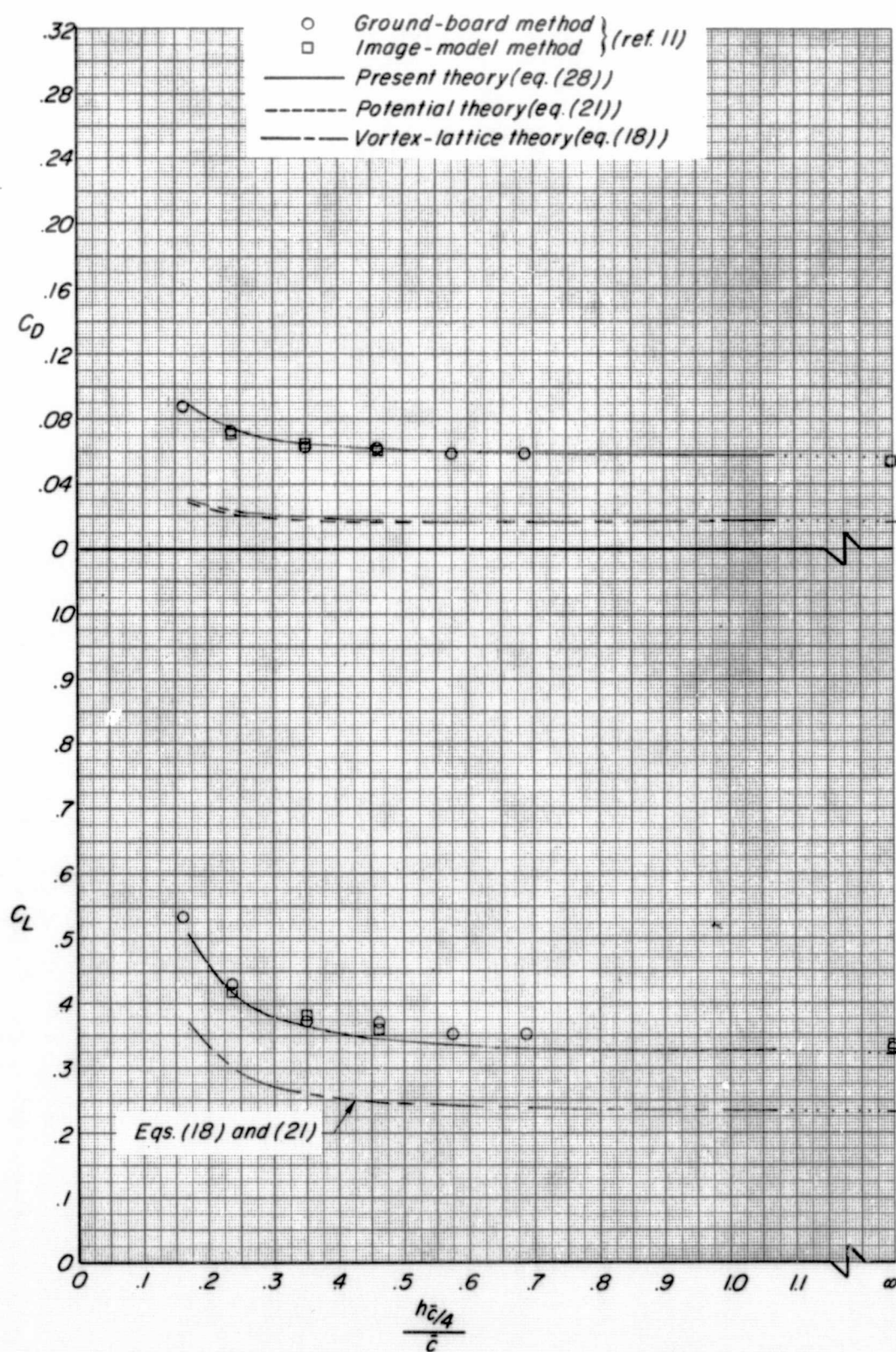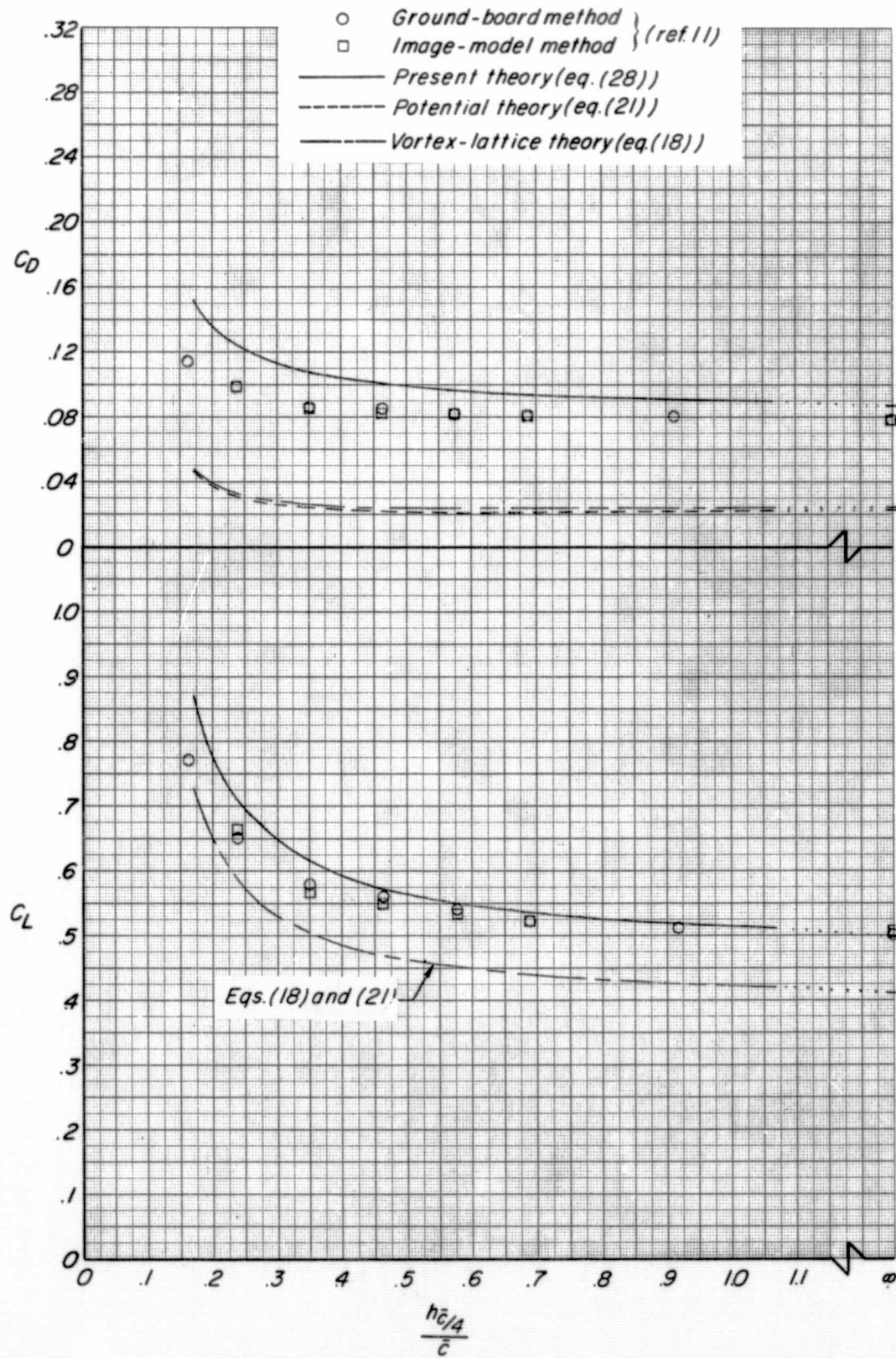
(a) $\Lambda = 75^{\circ}$; AR = 1.072.

Figure 4.- Comparison of lift and drag coefficients determined by
different theories with the experimental data of reference 11
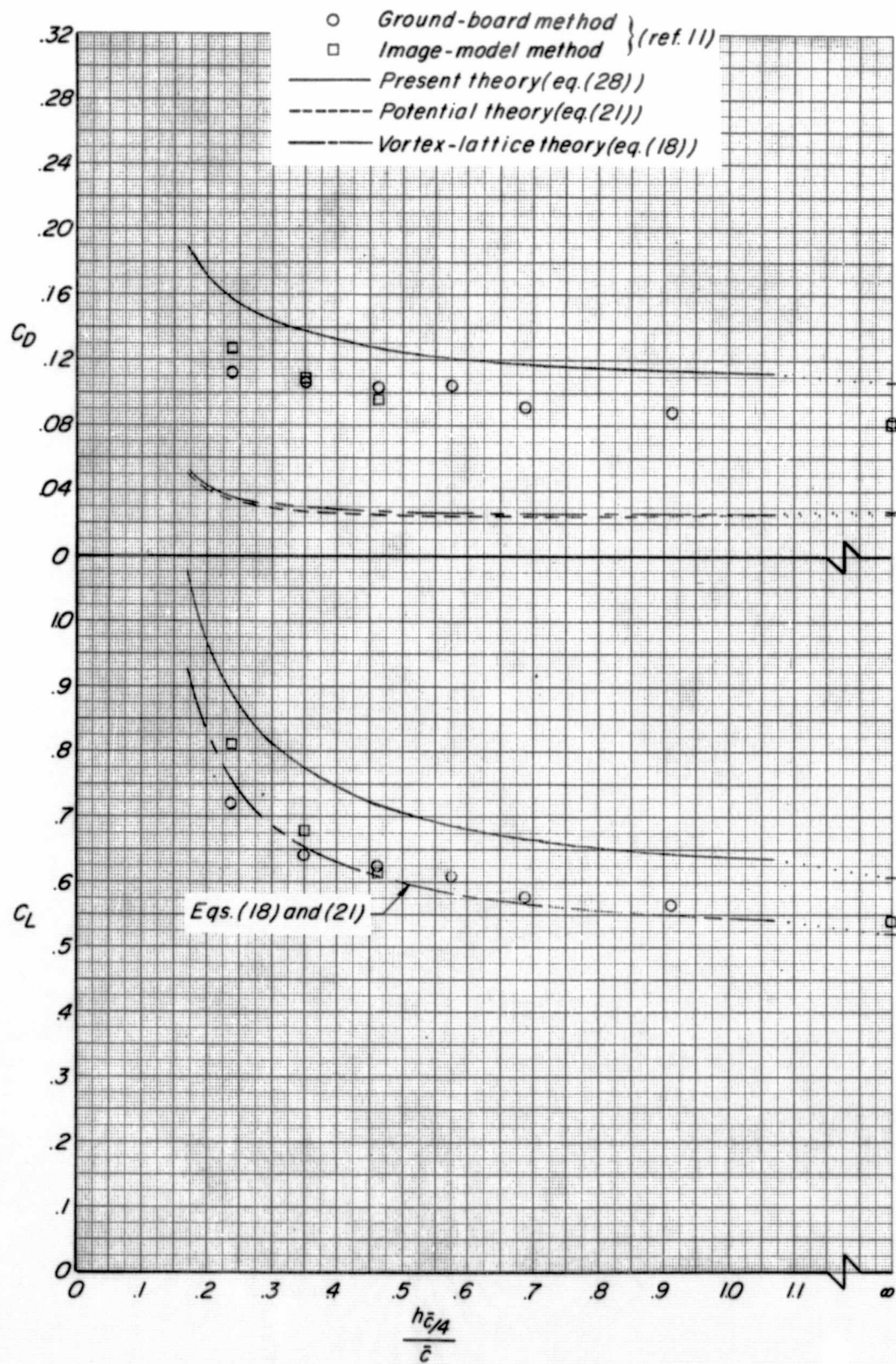at an angle of attack of 10°.
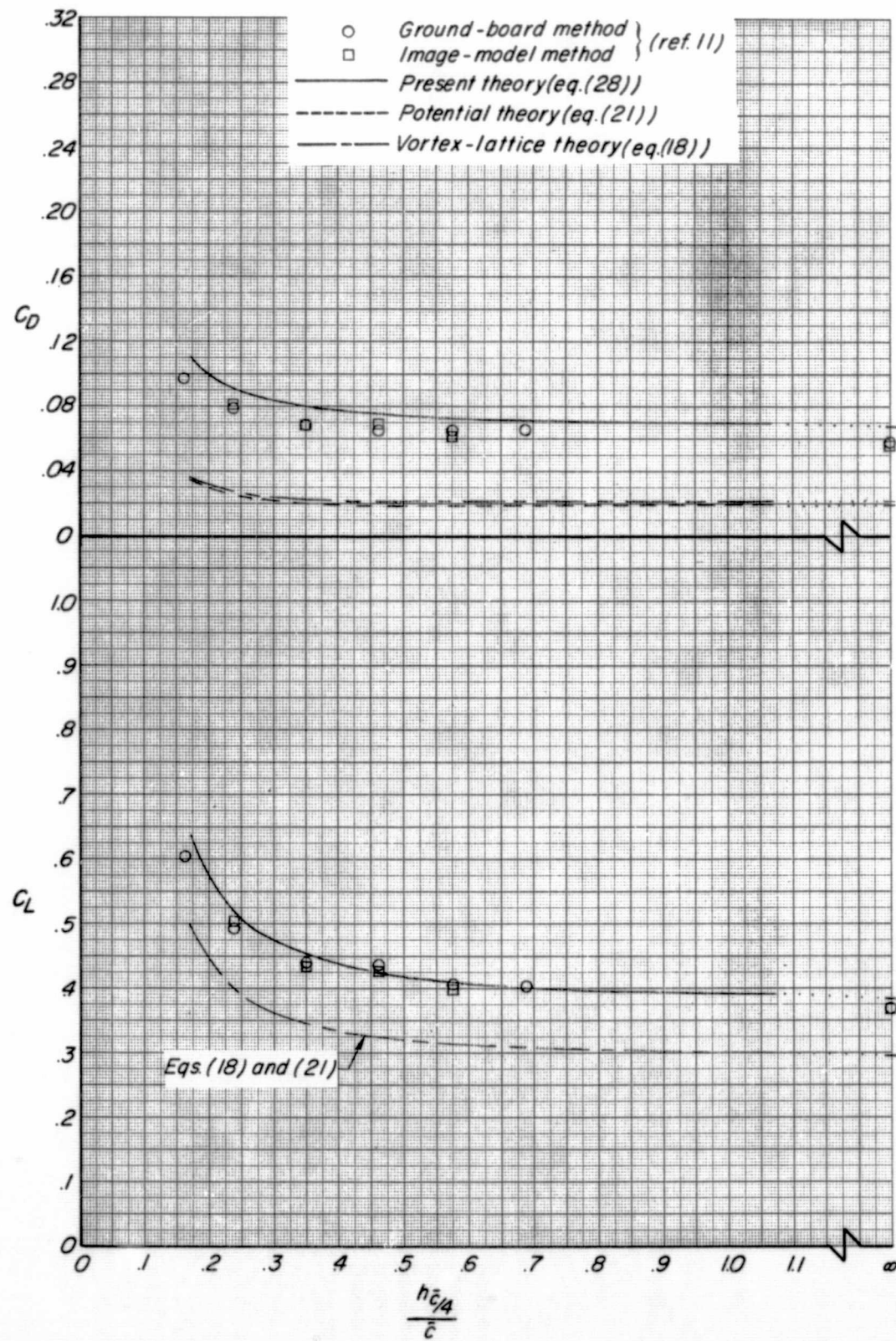
(b) $\Lambda = 70^\circ$; AR = 1.456.
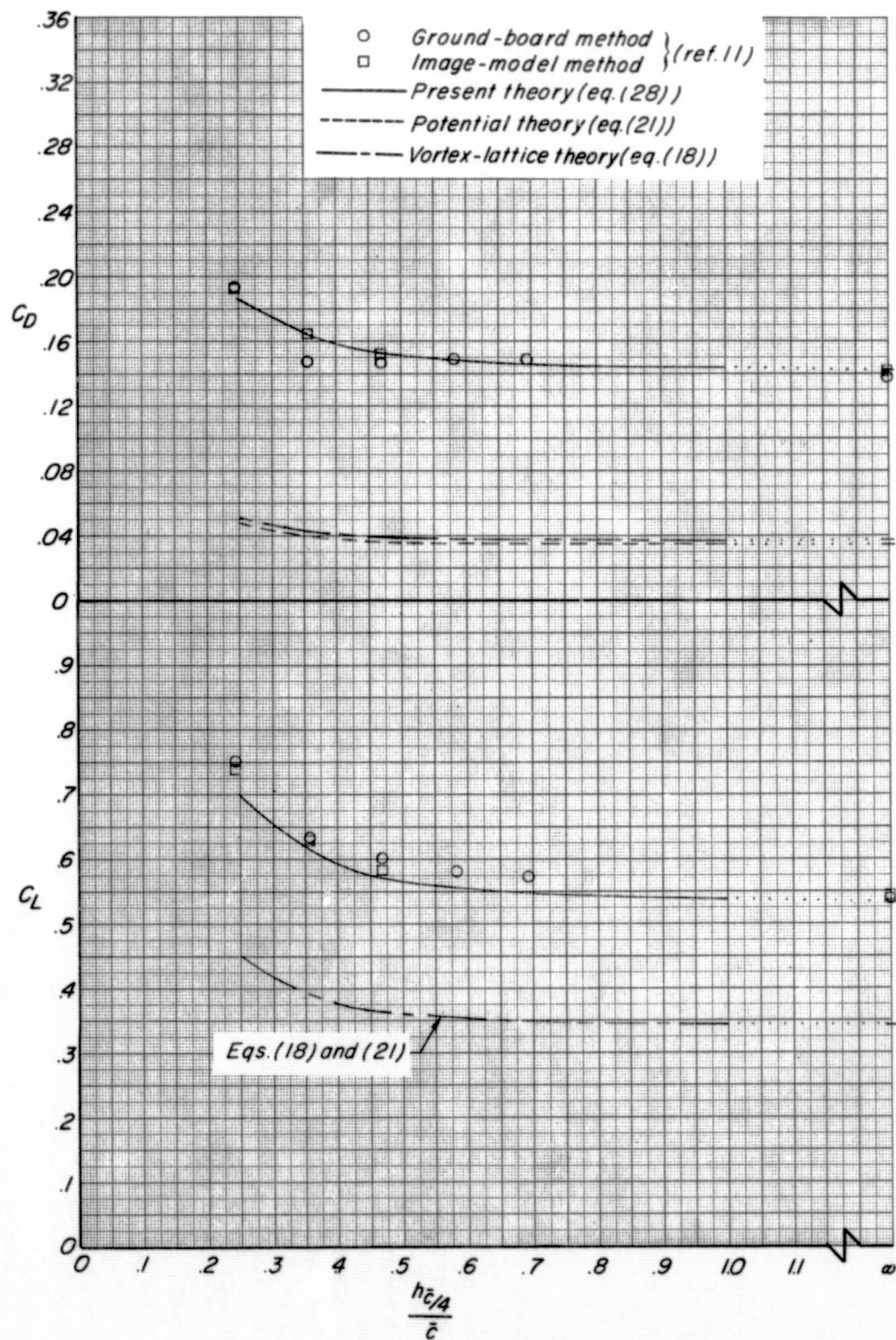
Figure 4.- Continued.
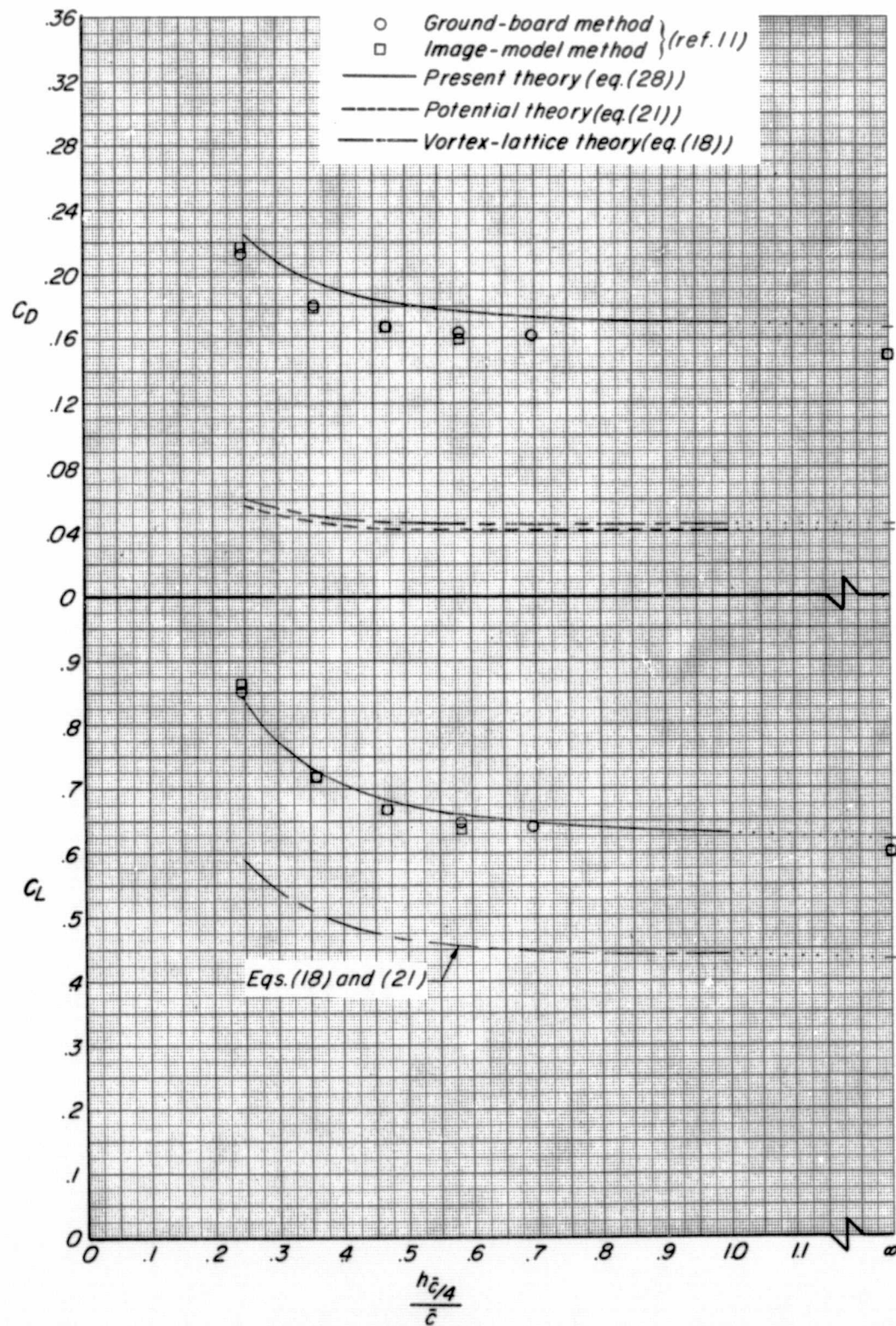
(c) $\Lambda = 60^\circ$; $AR = 2.309$.

Figure 4.- Continued:

(d) $\Lambda = 50^{\circ}$; AR = 3.356.
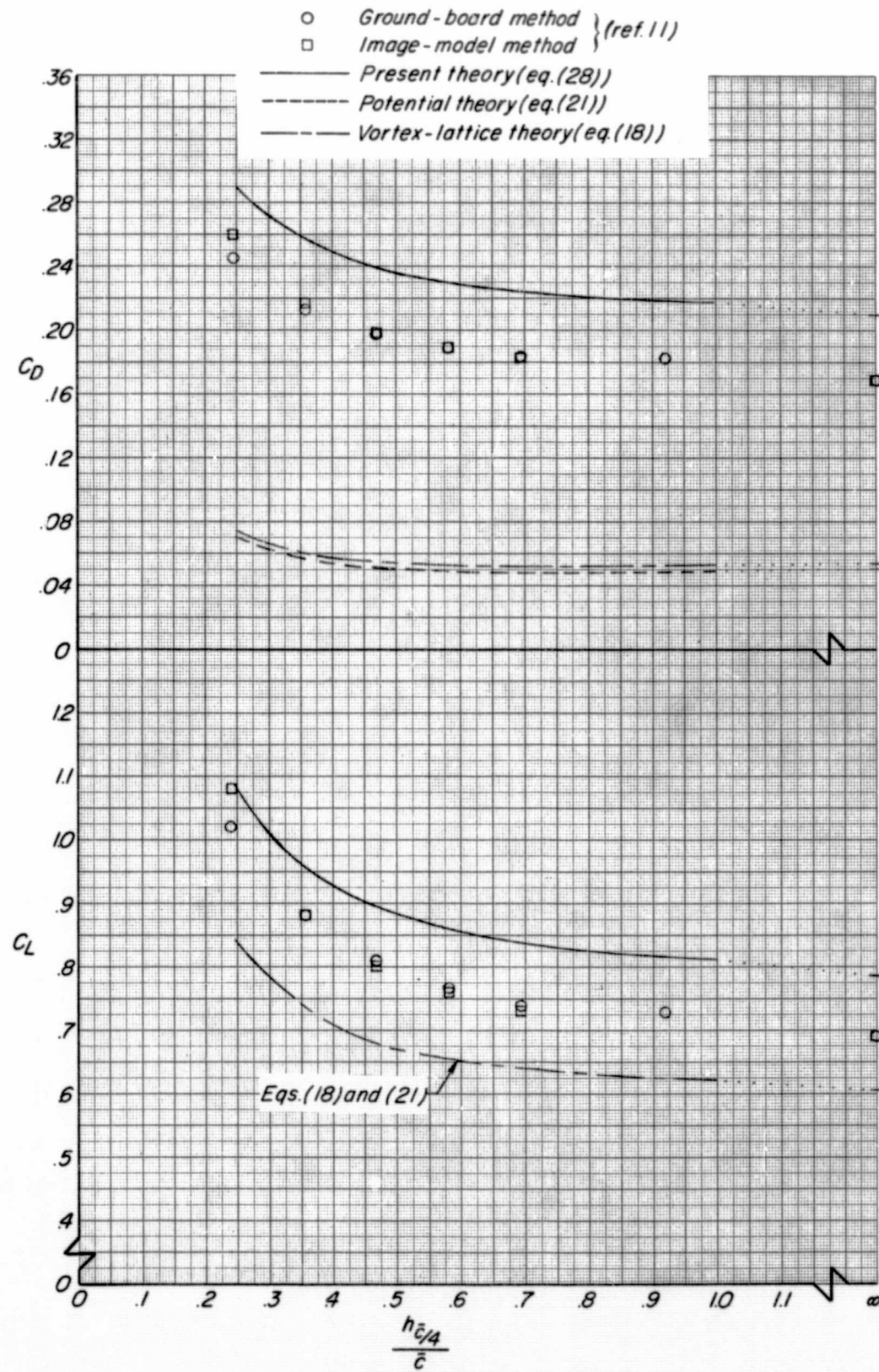
Figure 4.- Concluded.

(a) $\Lambda = 75^\circ$; AR = 1.072.

Figure 5.- Comparison of lift and drag coefficients determined by
   different theories with the experimental data of reference 11
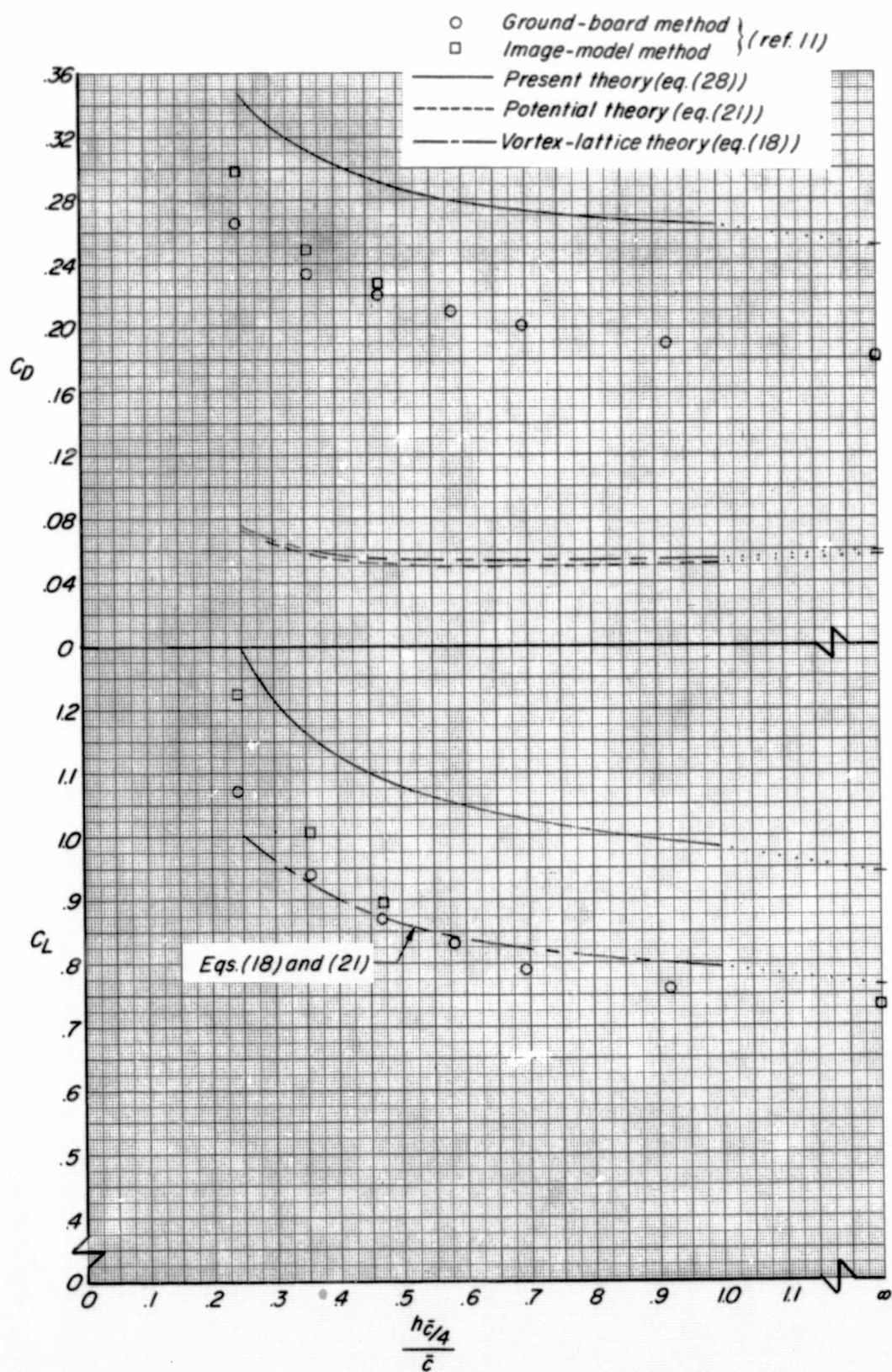   at an angle of attack of 15°.

(b) $\Lambda = 70^{\circ}$; $AR = 1.456.$

Figure 5.- Continued.

(c) $\Lambda = 60^\circ$; AR = 2.309.

Figure 5.- Continued.

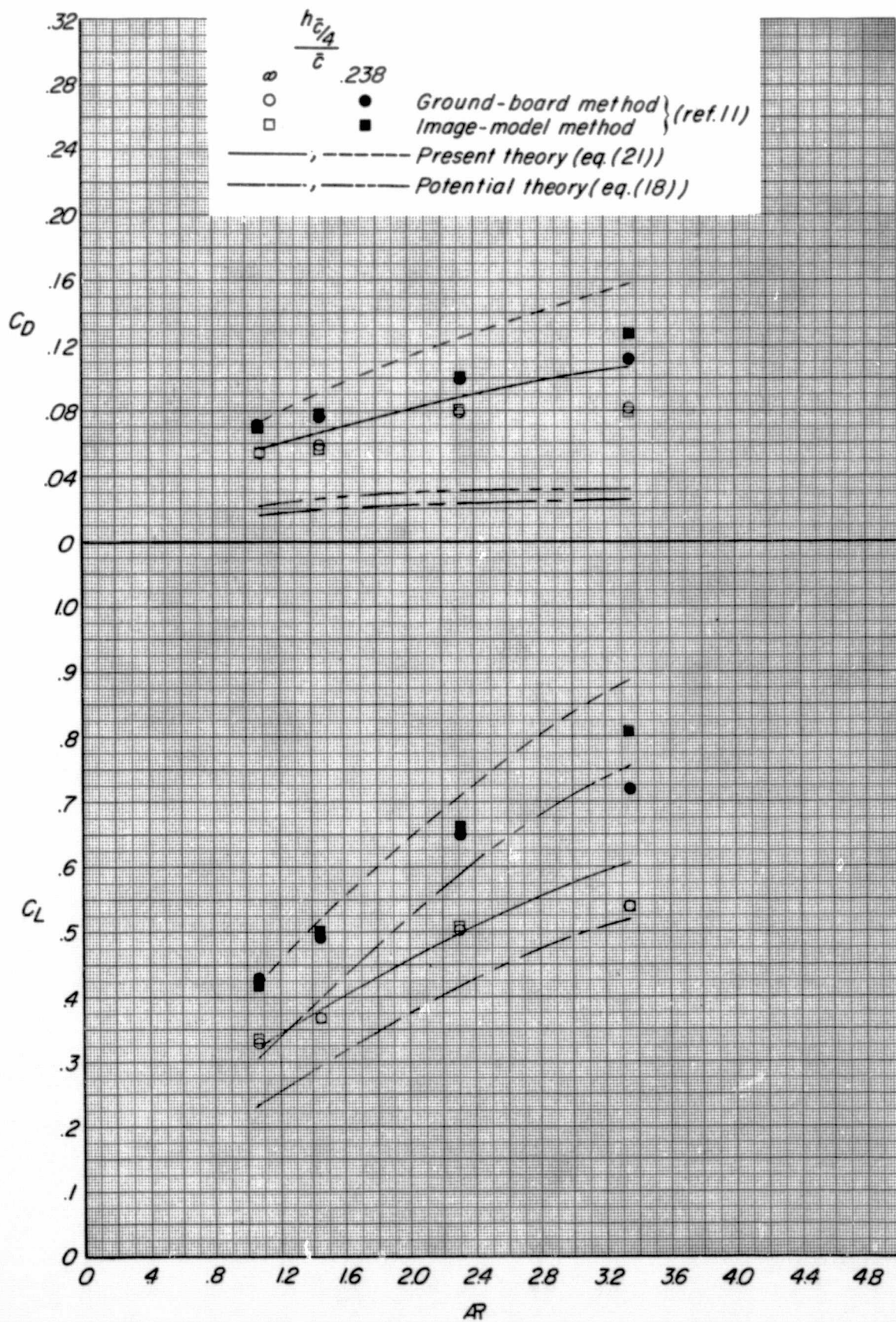(d) $\Lambda = 50^\circ$; AR =: 3.356.

Figure 5.- Concluded.

Figure 6.- Effect of aspect ratio on theoretical predictions of lift
and drag coefficients at two heights above the ground and
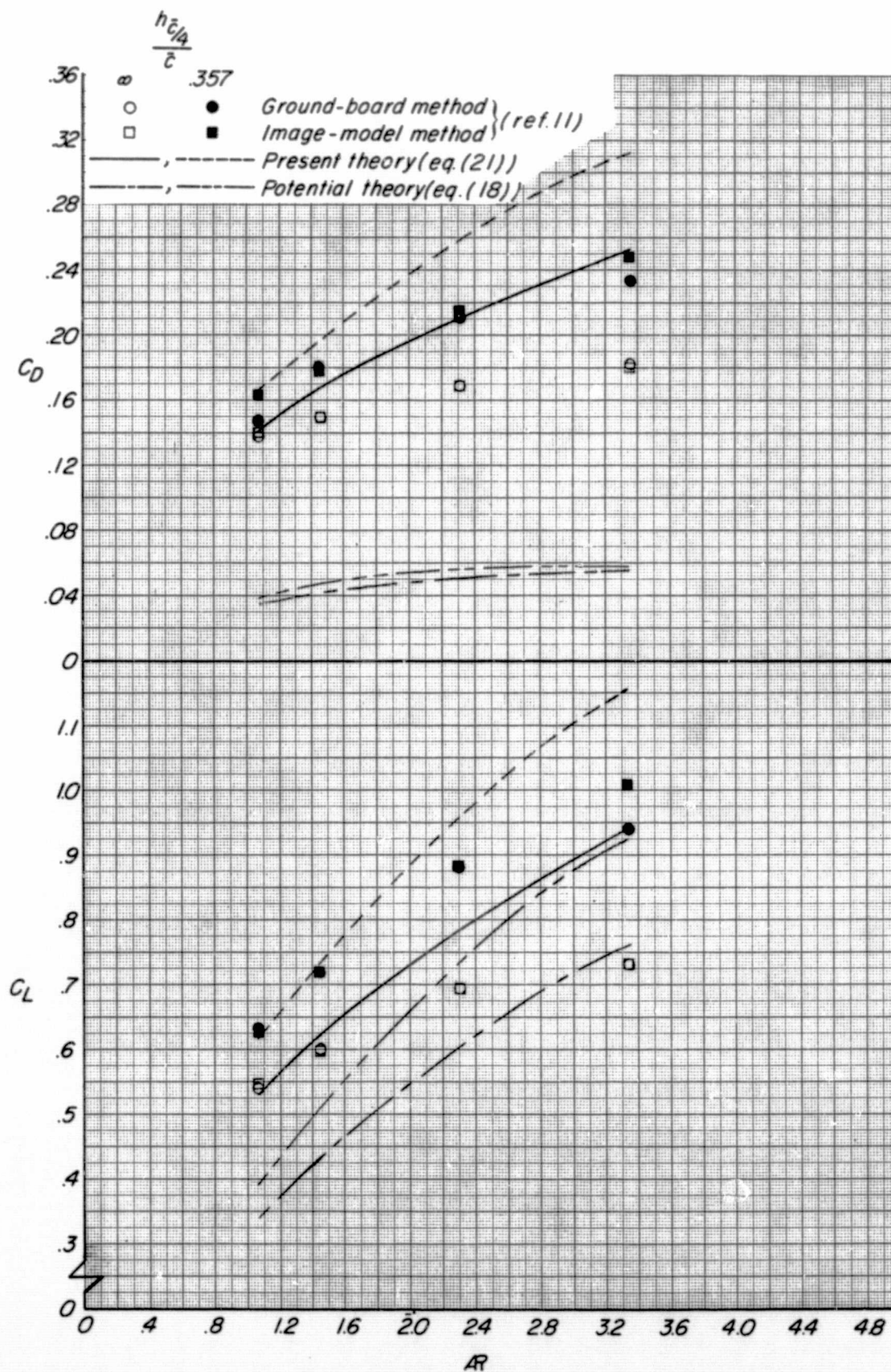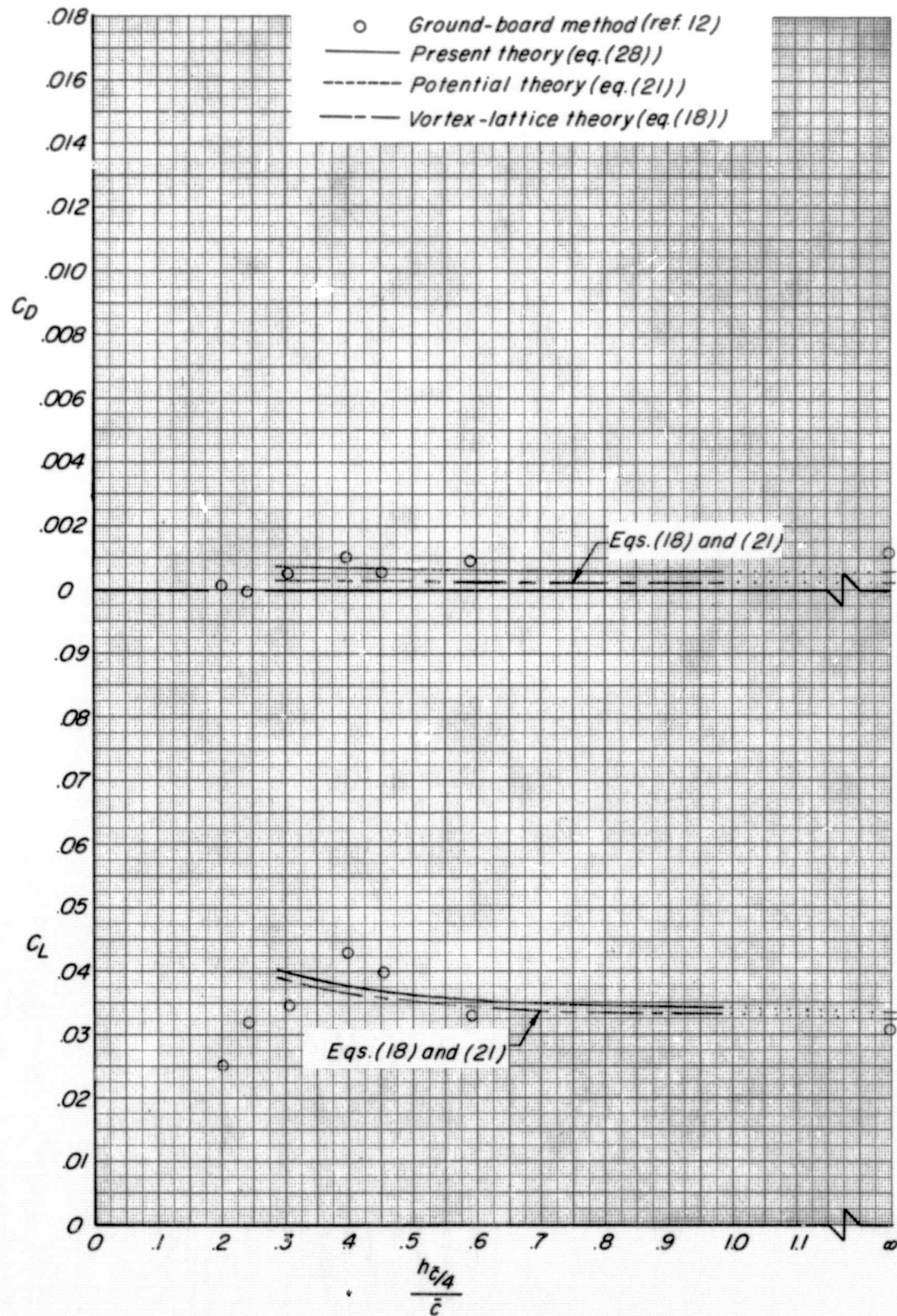comparison with experimental data of reference 11. $\alpha = 10°$.

Figure 7.- Effect of aspect ratio on theoretical predictions of lift and drag coefficients at two heights above the ground and comparison with experimental data of reference 11. $\alpha = 15°$.

In order to examine the effects of angle of attack over a larger range, the data of reference 12 were used. Reference 12 presents tabulated lift and drag data as functions of angle of attack and ground height for a wing with an aspect ratio of 1.616 ($\Lambda = 68^\circ$). The wing was suspended on a wire support rig over a fixed ground board and tested at a free-stream velocity of 120 ft/sec (36.6 m/sec). A minimum drag coefficient of 0.009 was subtracted from the measured drag data of reference 12 in order to compensate for the friction drag in the data.

The results of the theoretical calculations for a wing with an aspect ratio of 1.616 are compared with the data of reference 12 over an angle-of-attack range from 1° to 15.55° in figure 8. The comparison is further summarized in figure 9. Note that figures 6 and 7 indicate that the present theory should yield a good prediction of the lift and drag at this aspect ratio. The data from reference 12 indicate that the same result is obtained except at an angle of attack of 1°. It should be noted, however, that an angle of attack of 1° probably does not provide sufficient leading-edge separation for the complete formation of the leading-edge spiral-vortex system. Other than this anomalous point, the present theory gives a good prediction of the lift and drag for each angle of attack throughout the ground-height range. The predicted lift and drag are presented in figure 9 as a function of angle of attack for selected ground heights. The present theory yields a reasonably good prediction of the lift and drag throughout the angle-of-attack range from some angle of attack between 1° and 5.52° up to an angle of attack of 15.55°, the highest angle of attack for which experimental data were available. (See figure 8.)
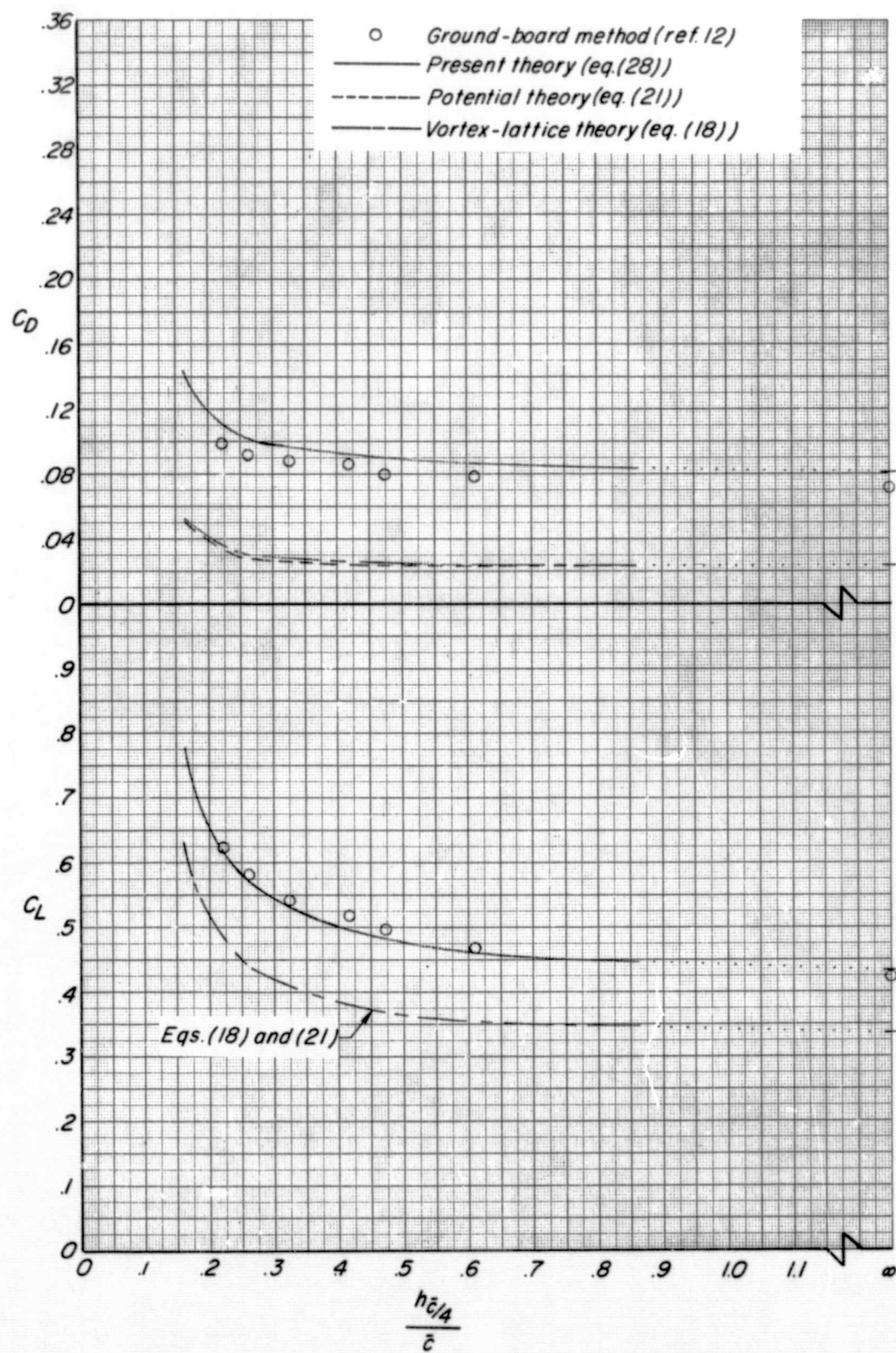
(a) $\alpha = 1^{\circ}$. Note the enlarged C_L and C_D scales.

Figure 8.- Comparison of lift and drag coefficients determined by different theories with the experimental data of reference 12. $\Lambda = 68^{\circ}$; AR = 1.616.
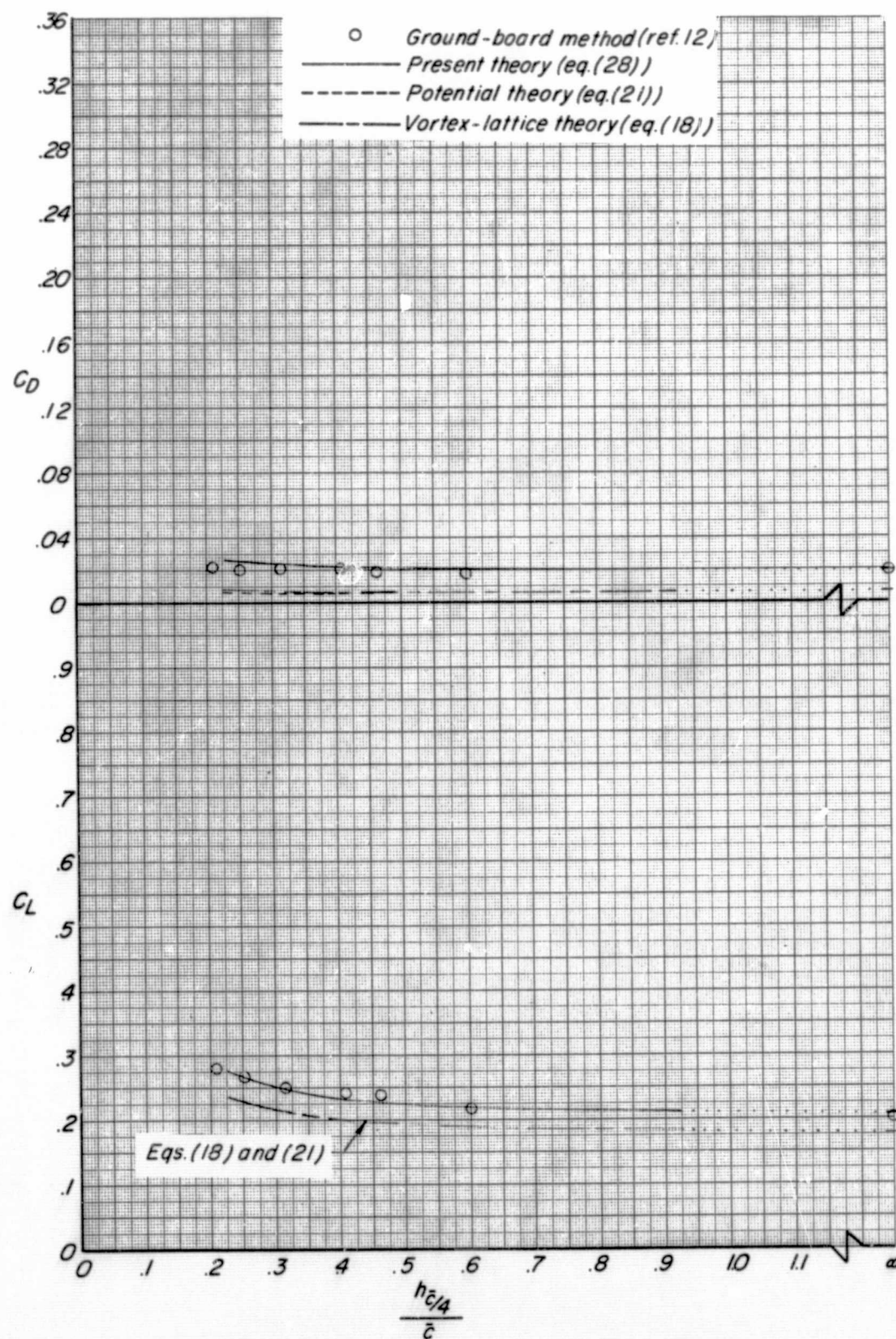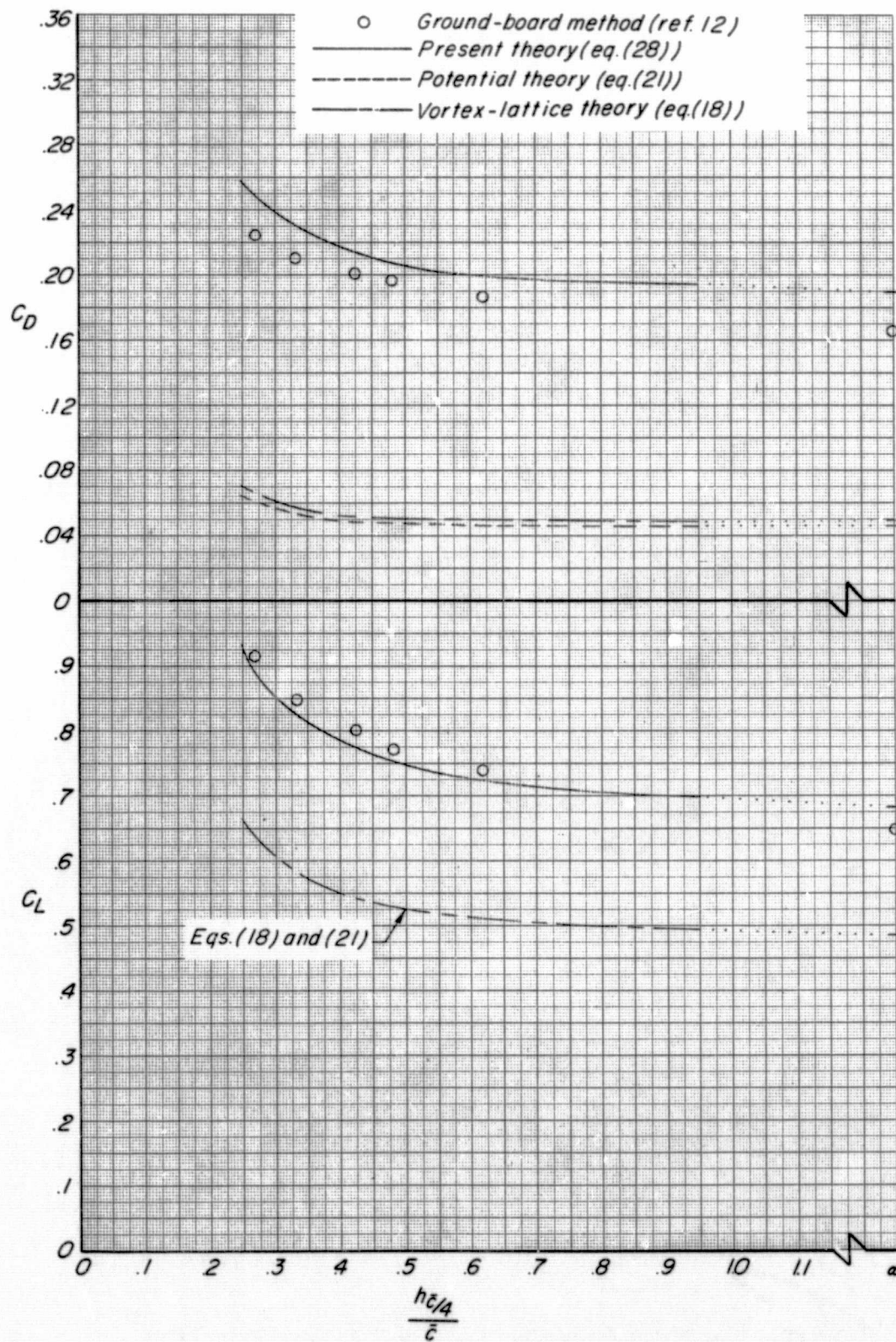
(b) $\alpha = 5.52°$.

Figure 8.- Continued.

(c) $\alpha = 10.53^\circ$.

Figure 8.- Continued.

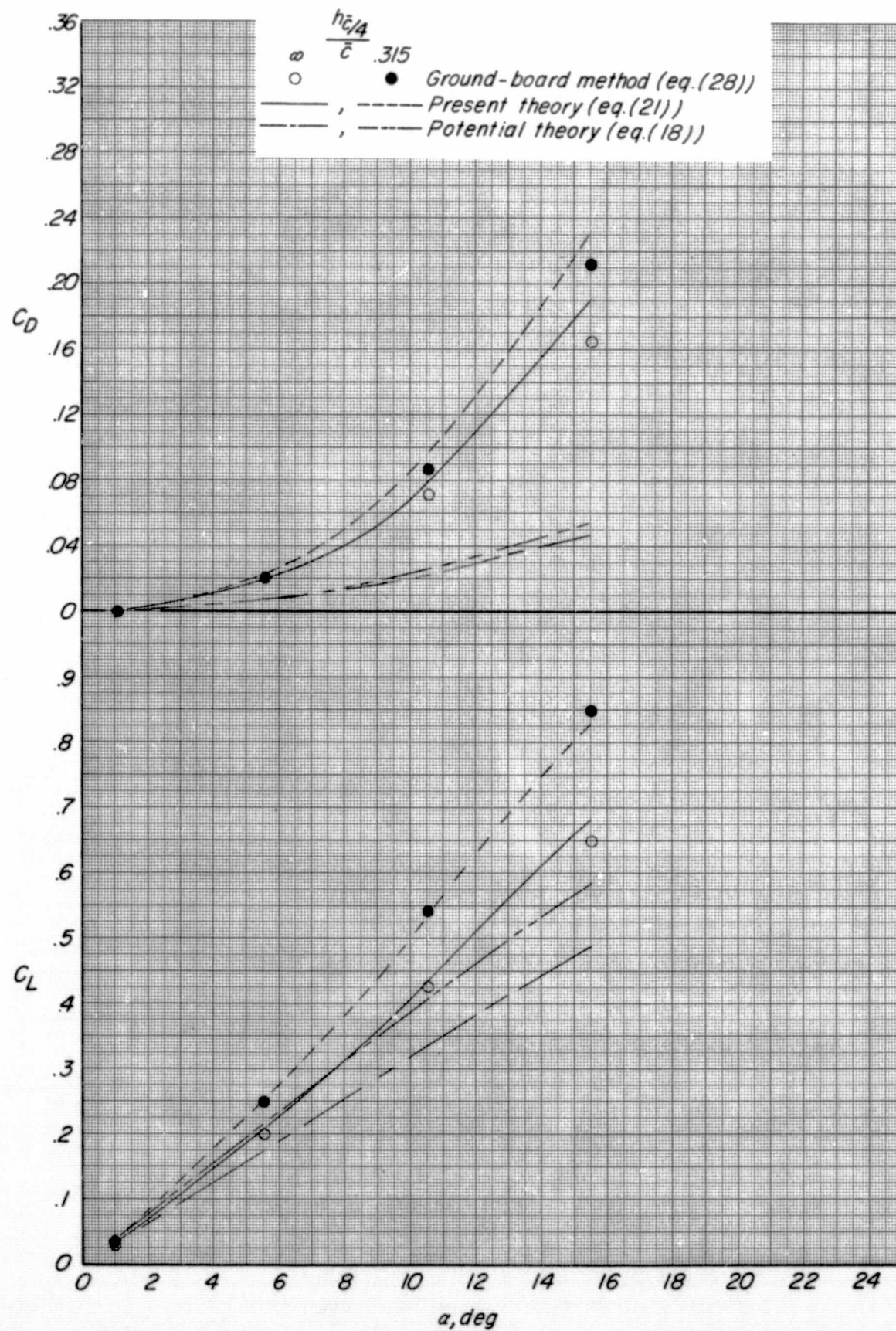(d) $\alpha = 15.55°$.

Figure 8.- Concluded.

Figure 9.- Effect of angle of attack on theoretical predictions of lift and drag coefficients at two heights above the ground and comparison with data of reference 12. $\Lambda = 68^\circ$; AR = 1.616.

The potential flow theory prediction, for the highest angle of attack presented in figure 9, is only 75 to 80 percent of the lift and 25 to 28 percent of the drag compared to a prediction by the present theory of 93 to 104 percent of the lift and 108 to 116 percent of the drag.

XI. <u>CONCLUDING REMARKS</u>

A method of predicting the lift and drag of slender planar sharp-edge delta wings in ground proximity is described, and the results are compared with experimental data. The method utilizes a vortex lattice method incorporating an image technique to compute the potential-flow normal-force and axial-force characteristics of delta wings in ground proximity. A correction to account for finite vortex-lattice spacing is made to the free-air vortex-lattice axial force, and the correction is assumed applicable to the vortex-lattice axial force in ground proximity. A recently published vortex lift concept in free air based on a leading-edge-suction analogy is utilized, and a method is presented for combining it with the results of the potential-flow theory in ground proximity. A comparison of the theoretical and experimental lift and drag is presented at selected angles of attack for delta wings with a wide range of aspect ratios. This method provides a reasonably good prediction of the lift and drag in ground proximity for aspect ratios less than 2.0 in the angle-of-attack range from approximately 5° to 16°.

XII. REFERENCES

1. Fox, Charles H., Jr.: Prediction of Lift and Drag for Slender Sharp-Edge Delta Wings in Ground Proximity. NASA TN D-4891, 1969.

2. Kemp, William B., Jr.; Lockwood, Vernard E.; and Phillips, W. Pelham: Ground Effects Related to Landing of Airplanes With Low Aspect Ratio Wings. NASA TN D-3583, 1966.

3. Campbell, George S.: A Finite-Step Method for the Calculation of Span Loadings of Unusual Plan Forms. NACA RM L50L13, 1951.

4. Rubbert, Paul E.: Theoretical Characteristics of Arbitrary Wings by a Nonplanar Vortex Lattice Method. The Boeing Company, document No. D6-9244, 1962.

5. Hedman, Sven G.: Vortex Lattice Method for Calculation of Quasi-Steady State Loadings on Thin Elastic Wings in Subsonic Flow. EFA rep. 105, Aeronaut. Res. Inst. Swed., 1966.

6. Polhamus, Edward C.: A Concept of the Vortex Lift of Sharp-Edge Delta Wings Based on a Leading Edge Suction Analogy. NASA TN D-3767, 1966.

7. Glauert, H.: The Elements of Aerofoil and Airscrew Theory. Second ed., Cambridge Univ. Press, 1947 (reprinted 1948).

8. Michels, Walter C., Ed.-in-Chief: The International Dictionary of Physics and Electronics. Second ed., D. Van Nostrand Co., Inc., 1961.

9. Lamb, Sir Horace: Hydrodynamics. Sixth ed., Dover Publications, 1945.

10. Lamar, John E.: A Modified Multhopp Approach for Predicting Lifting Pressures and Camber Shape for Composite Planforms in Subsonic Flow. NASA TN D-4427, 1968.

11. Anon.: Ailes Delta de Differentes Fleches et Aile Rectangulaire λ = 2 - Representation du Sol par la Methode du Plancher et par la Methode de 1 Image. O.N.E.R.A. P.V. No. 13/2449.A, October 1963.

12. Kirkpatrick, D. L. I.: Experimental Investigation of the Ground Effect on the Subsonic Longitudinal Characteristics of a Delta Wing of Aspect Ratio 1.616. Tech. Rep. No. 66179, Brit. R.A.E., June 1966.

XIII. VITA

The author was born in ████████████████ on ████████████████
He attended public schools in Camden and Clementon, New Jersey, and
graduated from Overbrook Regional High School in 1960. In 1965 he
received the degree of Bachelor of Science from Drexel Institute of
Technology with a major in physics. He has been employed by the National
Aeronautics and Space Administration at Langley Research Center, Langley
Station, Hampton, Virginia, from 1961 to 1965 as a Student Trainee and
since 1965 as an Aerospace Technologist.

Charles H. Fox, Jr.